Electron-impact ionization and recombination of *M*-shell atomic ions in the argon isonuclear sequence

S. D. Loch, Sh. A. Abdel-Naby, C. P. Ballance, and M. S. Pindzola
Department of Physics, Auburn University, Auburn, Alabama 36849, USA
(Received 20 December 2006; published 8 August 2007)

Electron-impact ionization and recombination cross sections and rate coefficients are calculated for *M*-shell Ar atomic ions using a configuration-average distorted-wave method. The electron-impact ionization calculations are for all atomic ions in the Ar isonuclear sequence. Ionization contributions include both direct ionization and excitation-autoionization processes. Good agreement is found between theory and experimental crossed-beam measurements for moderately charged ion stages. Comparisons are made with previous theoretical calculations where possible. We also generate rate coefficients for neutral argon ionization, based on recent *R*-matrix with pseudostates calculations. Electron-impact dielectronic recombination is calculated for all *M*-shell ions of argon. For Ar^{6+} and Ar^{7+} the current theoretical results agree well with previous level-resolved distorted-wave calculations. In order to compare with published ionization balance results our dielectronic recombination data are combined with literature values for the higher ion stages and with recent radiative recombination data for all the ion stages. We find significant differences in our equilibrium fractional abundances for the *M*-shell ions, compared with literature values. We relate these differences to the underlying atomic data.

DOI: 10.1103/PhysRevA.76.022706 PACS number(s): 34.80.Dp, 34.80.Lx, 52.20.Fs

I. INTRODUCTION

Over the years, due to its handling ease, argon has served as a valuable diagnostic element for magnetically controlled fusion plasmas [1,2]. Recently, the high-pressure gas-jet injection of argon and other rare gases has been shown to be a simple possible method for the mitigation of tokamak plasma disruptions [3]. The avoidance of major plasma disruptions is a key design issue in the future operation of the International Tokamak Experimental Reactor (ITER). Line ratios from the ions of Ar have also been shown to be accurate electron density and temperature diagnostics [4]. Abdallah and Clark [5] investigated the use of effective and explicit models in calculating the populations for all ion stages of argon. In particular they considered density-dependent effects on the population modeling. A detailed prediction of the line emission power spectrum from the various ion stages of argon relies on transport modeling and the accuracy of its underlying atomic collision physics. The atomic collision processes needed for tokamak transport modeling involve mainly electron-ion collisions and include excitation, ionization, and recombination. Of critical importance are accurate ionization and recombination rate coefficients for low ion stages of argon. In particular, using level-resolved distorted-wave methods to calculate dielectronic recombination for *M*-shell ions leads to prohibitively large calculations, with only the simpler Na-like and Mg-like sequences being possible, along with one recently published calculation on Al-like iron [6]. Thus, our main aim in this paper is to calculate dielectronic recombination for Al-like through to Cl-like argon using the configuration-average distorted-wave method and to determine what differences these data make to equilibrium ionisation balance calculations.

Electron-impact ionization cross sections and rate coefficients are calculated in a configuration-average distorted-wave approximation for Ar^{+}–Ar^{17+}. Theoretical cross sections for a number of these ion stages have not previously been published. The ionization contributions include both direct ionization and excitation-autoionization processes. Trends along the isonuclear sequence are investigated. We compare our configuration-average distorted-wave calculations with experimental crossed-beam measurements [7–18] for Ar^{+}–Ar^{7+}. We also compare with average-statistical distorted-wave calculations for Ar^{6+} [19] and with level-resolved distorted-wave calculations for Ar^{7+} [20]. To complete our isonuclear sequence study we generate rate coefficients for neutral argon based upon recent *R*-matrix with pseudostate ionization cross-section calculations [21].

In this paper, electron-impact dielectronic recombination cross sections and rate coefficients, for $\Delta n=0$ core excitations, are calculated in a configuration-average distorted-wave approximation for Ar^{+}–Ar^{7+}. From Ar^{+} to Ar^{5+} the open-shell nature of the atomic structure has made level-resolved distorted-wave calculations difficult for recombination cross sections and rate coefficients. However, we can compare our configuration-average distorted-wave calculations with recent level-resolved distorted-wave calculations [22,23] for Ar^{6+} and Ar^{7+}, providing a valuable check on our method. We note that storage-ring experimental measurements of recombination cross sections for all the *M*-shell ions from Ar^{+}–Ar^{7+} are still in the planning stages. For Ar^{8+}–Ar^{18+} we use previously published dielectronic recombination data calculated using a level-resolved distorted-wave method [24]. We also use radiative recombination data for all ion stages of argon from recent calculations [25].

With a consistent set of ionization and recombination rate coefficients in place, we then solved the collisional equations [26] for the equilibrium ion stage balance for Ar–Ar^{18+}. Comparisons are made with previous ion stage balance calculations [27,28] to determine the differences that our cross sections make to fractional abundance calculations.

The rest of the paper is organized as follows. In Sec. II we give a brief review of the configuration-average distorted-

wave theory as applied to electron-impact ionization and recombination processes. In Sec. III we compare our electron-impact recombination calculations with other calculations, where available. In Sec. IV we compare our electron-impact ionization calculations with experimental measurements and other calculations, where available. In Sec. V we compare our collisional ion stage balance calculations with other results. In Sec. VI we conclude with a brief summary. Unless otherwise stated, all quantities are given in atomic units.

II. CONFIGURATION-AVERAGE DISTORTED-WAVE THEORY

We present here a brief summary of configuration-average distorted-wave theory as applied to recombination and ionization processes. In the independent process approximation the total ionization cross section is given by

$$\sigma_{ion} = \sigma_{dion} + \sum_j \sigma^j_{exc} B^a_j, \tag{1}$$

where σ_{dion} is the direct ionization cross section and σ^j_{exc} is the excitation cross section to an autoionizing configuration j. The branching ratio for autoionization is given by

$$B^a_j = \frac{\sum_m A_a(j \to m)}{\sum_m A_a(j \to m) + \sum_n A_r(j \to n)}, \tag{2}$$

where A_a is an autoionization rate and A_r is a radiative rate. We neglect the resonant capture followed by a sequential double-autoionization process since it is generally a small fraction of the total ionization cross section and is confined to a small energy range below the upper excitation-autoionization thresholds. Also, even in cases where such multistep processes can be significant at a specific energy, they have a negligible effect on the total rate coefficient when they are convolved with the Maxwellian free-electron distribution.

In the independent process approximation the total recombination cross section is given by

$$\sigma_{rec} = \sigma_{drec} + \sum_j \sigma^j_{cap} B^r_j, \tag{3}$$

where σ_{drec} is the direct (radiative) recombination cross section and σ^j_{cap} is the resonant capture cross section to an autoionizing configuration j. The branching ratio for radiative stabilization is given by

$$B^r_j = \frac{\sum_m A_r(j \to m)}{\sum_m A_r(j \to m) + \sum_n A_a(j \to n)}. \tag{4}$$

Configuration-average expressions have been derived [29] for all cross sections and rates appearing in Eqs. (1)–(4). Configuration-average total ionization cross sections have been recently calculated for all atomic ions in the Kr [30] and W [31] isonuclear sequences, while configuration-average dielectronic recombination cross sections have been calculated for several atomic ions in the Li [32] isoelectronic sequence.

For direct ionization, a general transition between configurations has the form

$$(nl)^w k_i l_i \to (nl)^{w-1} k_e l_e k_f l_f \tag{5}$$

and the ionization cross section is given by

$$\sigma_{dion} = \int_0^{E/2} d\epsilon_e \frac{32w}{k_i^3 k_e k_f} \sum_{l_i,l_e,l_f} (2l_i+1)(2l_e+1)(2l_f+1) \times |M(nl,k_i l_i \to k_e l_e, k_f l_f)|^2, \tag{6}$$

where w is a subshell occupation number, nl are quantum numbers of the bound electron, $k_i l_i$, $k_e l_e$, and $k_f l_f$ are quantum numbers of the initial, ejected, and final continuum electrons, and the scattering matrix M is a sum over products of standard angular factors and radial direct and exchange electrostatic integrals.

For electron-impact excitation to autoionizing configurations, a general transition between configurations has the form

$$(n_1 l_1)^{w_1+1} (n_2 l_2)^{w_2-1} k_i l_i \to (n_1 l_1)^{w_1} (n_2 l_2)^{w_2} k_f l_f, \tag{7}$$

and the excitation cross section is given by

$$\sigma_{exc} = \frac{8\pi}{k_i^3 k_f} (w_1+1)(4l_2+3-w_2) \times \sum_{l_i,l_f} (2l_i+1)(2l_f+1) |M(n_1 l_1, k_i l_i \to n_2 l_2, k_f l_f)|^2, \tag{8}$$

where $n_1 l_1$ and $n_2 l_2$ are quantum numbers of the bound electrons and $k_i l_i$ and $k_f l_f$ are quantum numbers of the initial and final continuum electrons.

For direct (radiative) recombination, a general transition between configurations has the form

$$(nl)^{w-1} k_i l_i \to (nl)^w \tag{9}$$

and the recombination cross section is given by

$$\sigma_{drec} = \frac{16\pi\omega^3}{3k_i^3 c^3} (4l+3-w) \frac{2\max(l,l_i)}{(4l+2)(4l_i+2)} |D(k_i l_i \to nl)|^2, \tag{10}$$

where $\omega = \frac{k_i^2}{2} - \epsilon_{nl}$, c is the speed of light, and D is a radial dipole integral. Although radiative recombination cross sections may be readily calculated in the configuration-average approximation, we used the recent level-resolved distorted-wave results [25] in our solutions of the collisional equations for equilibrium ion stage balance.

For electron-impact capture to autoionizing configurations, a general transition between configurations may have the form

$$(n_1 l_1)^{w_1+1} (n_2 l_2)^{w_2-1} (n_3 l_3)^{w_3-1} k_i l_i \to (n_1 l_1)^{w_1} (n_2 l_2)^{w_2} (n_3 l_3)^{w_3} \tag{11}$$

and the resonant capture cross section is given by

$$\sigma_{cap} = \frac{2\pi}{k_i^3 \Delta\epsilon}(w_1+1)(4l_2+3-w_2)(4l_3+3-w_3) \times \sum_{l_i}(2l_i+1)|M(n_1l_1,k_il_i \rightarrow n_2l_2,n_3l_3)|^2. \quad (12)$$

Alternatively, a general transition between configurations may also have the form

$$(n_1l_1)^{w_1+1}(n_2l_2)^{w_2-2}k_il_i \rightarrow (n_1l_1)^{w_1}(n_2l_2)^{w_2} \quad (13)$$

and the resonant capture cross section is given by

$$\sigma_{cap} = \frac{2\pi}{k_i^3 \Delta\epsilon}(w_1+1)\frac{(4l_2+4-w_2)(4l_2+3-w_2)(4l_2+2)}{(4l_2+1)} \times \sum_{l_i}(2l_i+1)|M(n_1l_1,k_il_i \rightarrow n_2l_2,n_2l_2)|^2. \quad (14)$$

In the capture cross-section expressions, n_1l_1, n_2l_2, and n_3l_3 are quantum numbers of the bound electrons, k_il_i are quantum numbers for the initial continuum electrons, and $\Delta\epsilon$ is an energy width larger than the largest resonance width. This $\Delta\epsilon$ parameter provides a width that is used to bin the cross-section results. If the results are to be compared with an experiment, one would also need to include the experimental width. For the generation of Maxwellian rate coefficients the width of the Maxwellian distribution is much greater than the resonance width; thus, it is sufficient to choose a $\Delta\epsilon$ that is larger than the largest resonance width. For the calculations shown here a $\Delta\epsilon$ of 0.005 eV was used.

The energies and bound orbitals needed to evaluate all the configuration-average cross sections and rates appearing in Eqs. (1)–(4) are calculated in the Hartree-Fock relativistic (HFR) approximation [33], which includes the mass-velocity and Darwin corrections with modified HF differential equations. The continuum radial orbitals, with normalization chosen as one times a sine function, are obtained by solving a single-channel radial Schrodinger equation, which also includes the mass-velocity and Darwin corrections, where the distorting potential is constructed from HFR bound orbitals.

Convoluting the configuration-average distorted-wave cross sections with an isotropic Maxwellian electron temperature distribution yields a rate coefficient given by

$$\alpha(T_e) = \frac{2v_a}{\sqrt{\pi}}\sqrt{\frac{I_H}{T_e}}\int_0^\infty \frac{\epsilon}{I_H}\sigma(\epsilon)e^{-\epsilon/T_e}d\left(\frac{\epsilon}{T_e}\right), \quad (15)$$

where $v_a = 2.188 \times 10^8$ cm/s, $I_H = 13.60$ eV, ϵ is the energy in eV, T_e is the temperature in eV, $\sigma(\epsilon)$ is in cm^2, and $\alpha(T_e)$ is in cm^3/s.

III. IONIZATION CALCULATIONS

A. *M*-shell ions

The direct ionization of Ar^+–Ar^{5+} is enhanced by inner-shell excitations:

$$Ar^{(6-w)+}(2p^63s^23p^w) + e^- \rightarrow Ar^{(6-w)+}(2p^53s^23p^wnl) + e^-, \quad (16)$$

followed by autoionization, where $5 \leqslant w \leqslant 1$. We compare our configuration-average distorted-wave cross sections for Ar^+–Ar^{5+} with experimental crossed-beam measurements in Fig. 1. For Ar^+ in Fig. 1(a), the distorted-wave results overestimate the peak of the cross section, but are in reasonable agreement with experimental measurements [7,8] at the higher energies. For Ar^{2+} in Fig. 1(b), there is reasonable agreement between the distorted-wave results and the experimental measurements of Man *et al.* [9]. The measurements of Danjo *et al.* [10] and Mueller *et al.* [11] have cross sections below the Ar^{2+} ground ionization potential, indicating metastable fractions in these experiments. This is also consistent with fact that these measured cross sections are larger than the measurements of Man *et al.* [9]. For Ar^{3+} in Fig. 1(c), the distorted-wave results are slightly higher than the experimental measurements [12,13] at the peak of the cross section but are in good agreement at higher energies. The experimental measurements show no ionization cross section below the ground ionization potential and are close to the configuration-average distorted-wave direct ionization results near threshold. It may be that the levels of an autoionizing configuration are split such that they span the ionization threshold, leading to an overestimation of the total cross section in our configuration-average calculation. For Ar^{4+} in Fig. 1(d), there is good agreement between the distorted-wave results and the experimental measurements of Müller *et al.* [12] and Zhang *et al.* [14]. For Ar^{5+} in Fig. 1(e), there is good agreement between the distorted-wave results and the experimental measurements of Crandall *et al.* [15]. The other measurements of Müller *et al.* [12] and Zhang *et al.* [14] are in agreement with each other, with the measurements of Müller *et al.* [12] showing an ionization cross section below the Ar^{5+} ground ionization potential, indicating a possible metastable fraction.

The direct ionization of Ar^{6+} is enhanced by inner-shell excitations:

$$Ar^{6+}(2p^63s^2) + e^- \rightarrow Ar^{6+}(2p^53s^2nl) + e^-, \quad (17)$$

followed by autoionization. We compare our configuration-average distorted-wave cross sections with experimental crossed-beam measurements [14,16] in Fig. 2(a). When examined on a finer energy scale, the near-threshold region in Fig. 2(a) shows that there is a significant metastable fraction in both experiments. Term-resolved *R*-matrix [34] calculations have previously been performed for the excitation-autoionization contribution of Ar^{6+}. Also, average-statistical calculations [19], using level-resolved energies for the autoionizing levels, have been performed for the $2p^63s^2$ ground configuration and the $2p^63s3p$ excited configuration. This latter calculation showed that good agreement between theory and experiment was only achieved when the $2p^63s3p$ excited configuration, with metastable terms, was considered. Our configuration-average distorted-wave total cross section for the ground configuration is in good agreement with the average statistical results. Thus, we still expect the configuration-average distorted-wave results to be accurate for ionization from the ground state of Ar^{6+}.

The direct ionization of Ar^{7+} is enhanced by inner-shell excitations:

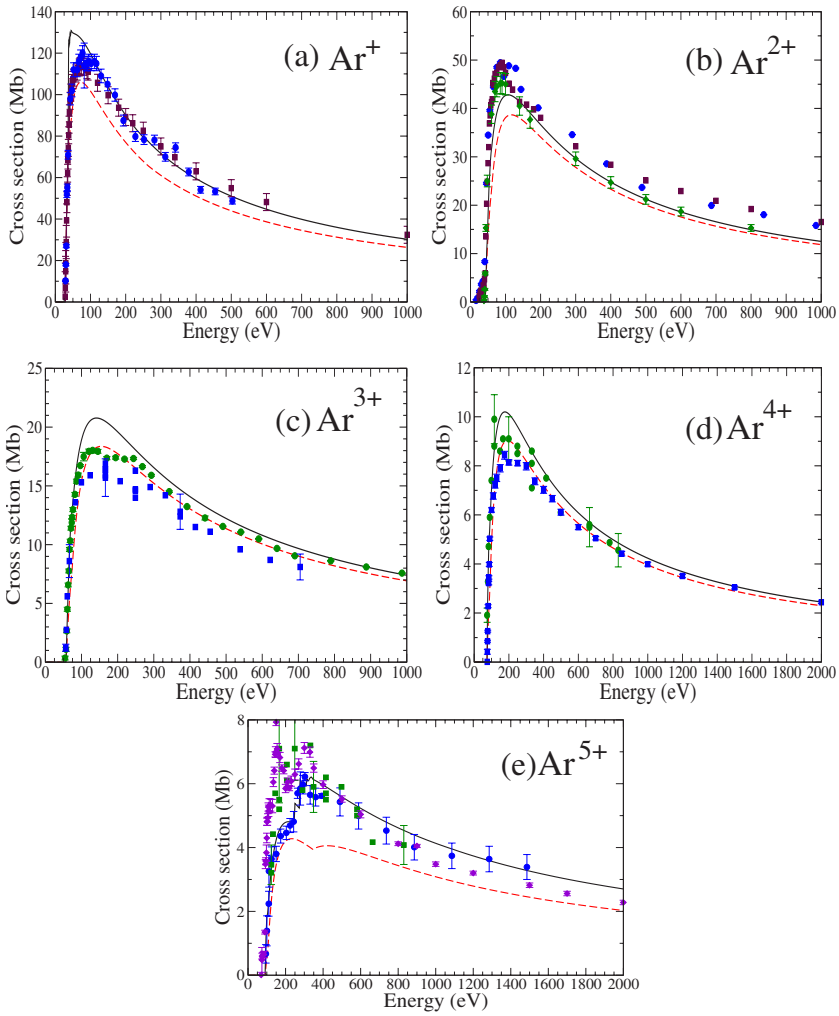

FIG. 1. (Color online) Electron-impact ionization cross sections: solid curve, total cross section; dashed curve, direct cross section only. (a) Ar^{+}: solid squares, experiment [7]; solid circles, experiment [8]. (b) Ar^{2+}: solid diamonds, experiment [9]; solid squares, experiment [10]; solid circles, experiment [11]. (c) Ar^{3+}: solid circles, experiment [13]. (d) Ar^{4+}: solid circles, experiment [12]; solid squares, experiment [14]. (e) Ar^{5+}: solid squares, experiment [12]; solid diamonds, experiment [14]; solid circles, experiment [15] (1.0 Mb $=1.0\times10^{-18}$ cm^2).

$$Ar^{7+}(2p^6 3s) + e^- \rightarrow Ar^{7+}(2p^5 3snl) + e^-, \qquad (18)$$

followed by autoionization. We compare our configuration-average distorted-wave cross sections with experimental crossed-beam measurements [17] in Fig. 2(b). We find good agreement between theory and experiment over the entire energy range. We do not show the measurements of Rachafi *et al.* [18], which are consistently lower than the measurements of Zhang *et al.* [17]. Our configuration-average cross sections are in excellent agreement with level-resolved distorted-wave results calculations [20], providing a useful check on our method.

B. *L*-shell ions

Direct ionization dominates the total ionization cross section for Ar^{8+} and higher ionization stages. Our configuration-average distorted-wave cross sections are in good agreement for the *L*-shell ion stages for which experiments exist: namely, Ar^{8+}, Ar^{10+}, and Ar^{11+}. The cross-section results are not shown, but are available from the authors upon request.

IV. RECOMBINATION CALCULATIONS

A. *M*-shell ions

The dielectronic recombination for $\Delta n=0$ excitation of Ar^{+}–Ar^{5+} occurs via the intermediate autoionizing configurations:

$$\begin{aligned} Ar^{(6-w)+}(3s^2 3p^w) + e^- &\rightarrow Ar^{(5-w)+}(3s^2 3p^{w-1} 3dnl) \\ &\rightarrow Ar^{(5-w)+}(3s3p^{w+1}nl) \\ &\rightarrow Ar^{(5-w)+}(3s3p^w 3dnl), \end{aligned} \qquad (19)$$

where $5 \leqslant w \leqslant 1$. In our calculations n and l are included explicitly up to $n=10$ and $l=7$, while extrapolations are used to include contributions up to $n=1000$ and $l=12$. The magnitudes of the $3s \rightarrow 3p$ and $3s \rightarrow 3d$ excitations were found to be very much smaller than the $3p \rightarrow 3d$ excitations at the temperatures relevant for plasmas dominated by electron collisions and, therefore, were not included in our total recombination rate coefficients. Higher $\Delta n=1$ excitations were not considered, since they were found to also be very small compared to $\Delta n=0$ excitations in recent level-resolved distorted-wave calculations for Al-like Fe^{13+} [6]. We present our configuration-average distorted-wave rate coefficients for Ar^{+}–Ar^{5+} in Fig. 3. There are no quantum mechanically derived rate coefficients to compare with for these ion stages. Hence, we extended our configuration-average distorted-wave calculations to Ar^{6+} and Ar^{7+} to provide a comparison of our method with previously published level-resolved distorted-wave calculations.

The dielectronic recombination for $\Delta n=0$ excitation of Mg-like Ar^{6+} occurs via the intermediate autoionizing configurations:

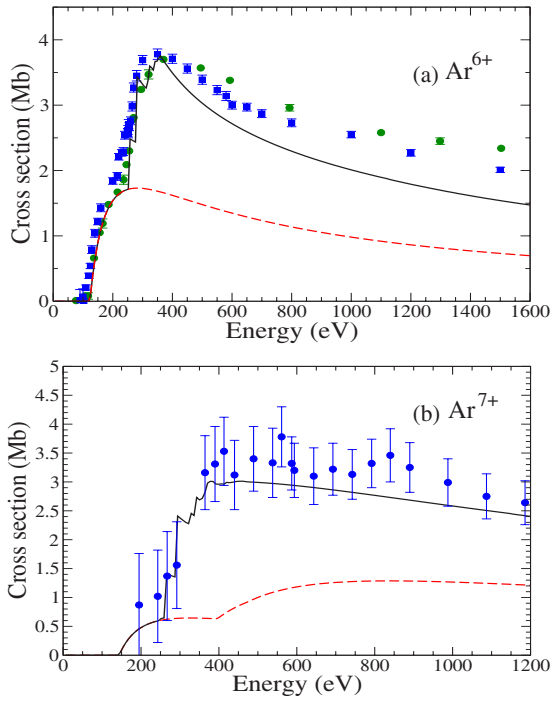

FIG. 2. (Color online) Electron-impact ionization cross sections: solid curve, total cross section; dashed curve, direct cross section only. (a) Ar^{6+}: solid squares, experiment [14]; solid circles, experiment [16]. (b) Ar^{7+}: solid circles, experiment [17] (1.0 Mb=1.0 $\times 10^{-18}$ cm^2).

$$Ar^{6+}(3s^2) + e^- \rightarrow Ar^{5+}(3s3pnl) \rightarrow Ar^{5+}(3s3dnl), \quad (20)$$

where we have used the same values for n and l as we did in the Ar^+ to Ar^{5+} cases. We compare our configuration-average distorted-wave rate coefficients with level-resolved distorted-wave calculations [22] in Fig. 4(a). The large differences at low temperatures are due to differences in the near threshold resonances in the two calculations. The small differences at high temperatures are due to term splitting of the core-excited energies of the $3s3p$ and $3s3d$ excited configurations which are not accounted for in the configuration-average calculations. As will be shown in Sec. V, for plasmas dominated by electron collisions, the Ar^{6+} ion stage balance will be mainly determined by the values of the recombination rate coefficients above 10 eV.

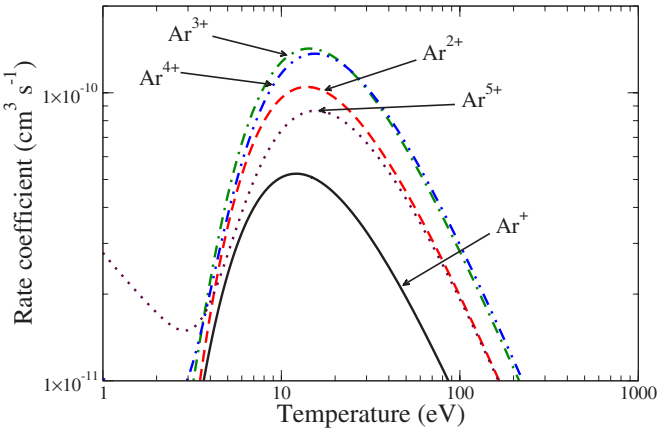

FIG. 3. (Color online) Dielectronic recombination rate coefficients. Solid line, Ar^{5+}; dashed line, Ar^{4+}; dotted line, Ar^{3+}; dot-dashed line, Ar^{2+}; double-dot-dashed line, Ar^+.

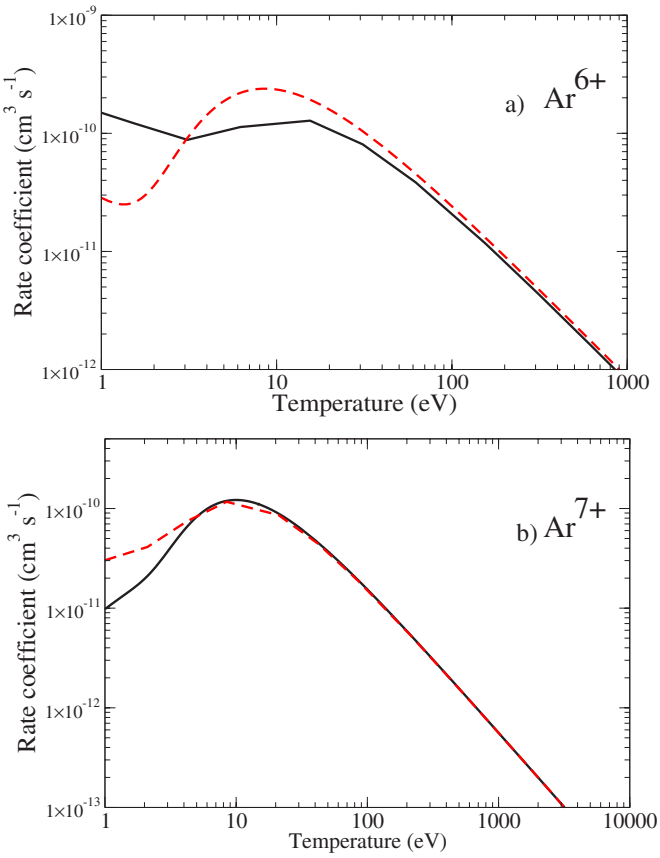

FIG. 4. (Color online) Dielectronic recombination rate coefficients. (a) Ar^{6+}: solid line, configuration-average distorted-wave; dashed line, level-resolved distorted-wave [22]. (b) Ar^{7+}: solid line, configuration-average distorted-wave; dashed line, level-resolved distorted-wave [23].

The dielectronic recombination for $\Delta n=0$ excitation of Na-like Ar^{7+} occurs via the intermediate autoionizing configurations:

$$Ar^{7+}(3s) + e^- \rightarrow Ar^{6+}(3pnl) \rightarrow Ar^{6+}(3dnl), \quad (21)$$

where we have used the same values for n and l as we did in the Ar^+–Ar^{6+} cases. We compare our configuration-average distorted-wave rate coefficients with level-resolved distorted-wave calculations [23] in Fig. 4(b). At low temperatures there is a large disagreement between the configuration-average and level-resolved distorted-wave calculations. This is due to the fact that the energy for the $3d4f$ configuration is bound, while some of the energy levels of the $3d4f$ configuration are actually autoionizing. A few levels just above the ionization limit can have a large effect on the recombination rate for low temperatures. On the other hand, there is very good agreement between the configuration-average and level-resolved distorted-wave calculations at high temperatures. As will be shown in Sec. V, for plasmas dominated by electron collisions, the Ar^{7+} ion stage balance will be mainly

determined by the values of the recombination rate coefficients above 20 eV.

The comparison between our configuration-average distorted-wave results and the level-resolved distorted-wave results gives us increased confidence in the configuration average results for the lower ion stages. The results for the lower ion stages also provides an indication of the most important recombining channels, to guide future level-resolved calculations.

B. *K*- and *L*-shell ions

To complete our recombination data, we take all of our dielectronic recombination data for the *K*- and *L*-shell ions from calculations of the DR project [24]. This has been a project aimed at the calculation of large quantities of dielectronic recombination data for a range of isoelectronic sequences. Our radiative recombination data are taken from the recent work of Badnell [25].

V. ION-STAGE BALANCE CALCULATIONS

Since our dielectronic recombination cross section for Ar^{+}–Ar^{5+} are potentially very different from the semiempirical data used in current modeling codes, we wish to determine the effect of our current data on equilibrium fractional abundance calculations. We solve the following system of collisional equations:

$$\frac{dN^z}{dt} = N_e S^{z-1\to z} N^{z-1} - N_e (S^{z\to z+1} + R^{z\to z-1}) N^z + N_e R^{z+1\to z} N^{z+1}, \tag{22}$$

where N^z is the population of each Ar ion stage. Here $S^{z-1\to z}$ represents the ionization rate coefficient from ion stage $z-1$ into z and $R^{z\to z-1}$ represents the total recombination rate coefficient from ion stage z into $z-1$. We use the configuration-average distorted-wave results found in Sec. III for the electron recombination of Ar^{+}–Ar^{7+}, supplemented by level-resolved distorted-wave results for Ar^{8+}–Ar^{18+} [24,25,35–43]. We use the configuration-average distorted-wave results found in Sec. IV for the electron ionization of Ar^{+}–Ar^{17+}, supplemented by recent *R*-matrix pseudostate results for neutral Ar [21].

We solve for the equilibrium ionization balance results by setting all of the $\frac{dN^z}{dt}$ terms to zero, so that we can compare to literature values for fractional abundances. We note that in relatively dense dynamic plasma conditions, such as those found in tokamak plasmas, one must account for a dynamic ionization balance while also allowing for ionization from metastable and excited states and for plasma transport effects. We compare to the work of Mazzotta *et al.* [27] and Bryans *et al.* [28], as the equilibrium ionization balance is of particular relevance to a wide range of astrophysical plasmas. The work of Bryans *et al.* [28] uses the same ionization data as that of Mazzotta *et al.* [27], but replaces the dielectronic recombination data with that from recent literature.

Ion-stage fractional abundances as a function of electron temperature for Ar–Ar^{8+} are shown in Fig. 5. We show the

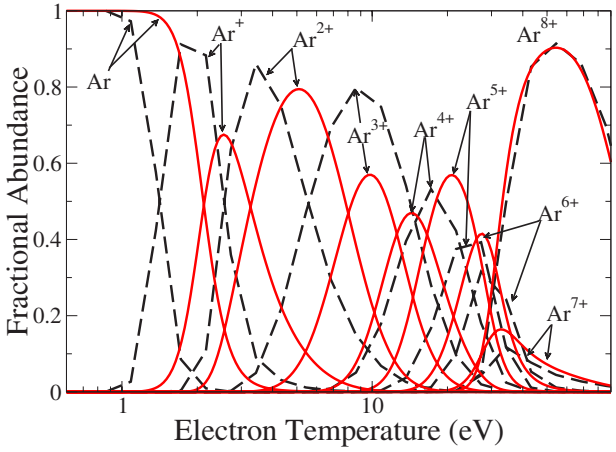

FIG. 5. (Color online) Equilibrium ion-stage balance for Ar–Ar^{8+}. Solid line, our distorted-wave atomic data; dashed line, older atomic data [27].

results using our distorted-wave ionization and recombination data and compare with the tabulated fractional abundances of Mazzotta *et al.* [27]. It can be seen that there are significant differences between the two sets of results. Both calculations show a similar abundance for Ar^{8+}, but many of the rest of the peaks are shifted in both temperature and height. The differences in the neutral argon and Ar^{+} abundances are due to the *R*-matrix with psuedostate ionization rate coefficient in our calculation, and to the configuration-average distorted-wave dielectronic recombination data for Ar^{+} recombining into neutral Ar. As shown by Ballance *et al.* [21] the *R*-matrix with psuedostate ionization cross section for neutral argon is significantly lower than the distorted-wave cross section. Hence the our neutral argon ionization rate coefficient will be smaller than that of Mazzotta *et al.* [27], allowing the neutral argon ion stage to exist up to a higher temperature in our calculation. The differences in the Ar^{2+}–Ar^{5+} abundances are largely due to differences in the underlying dielectronic recombination data. Mazzotta *et al.* [27] take their dielectronic recombination data from a range of sources, including the semiempirical Burgess-Mertz formula. Thus it is not possible to evaluate which resonant features in the dielectronic recombination lead to the differences in our recombination data. We note that the fractional abundances for Ar–Ar^{8+} from Bryans *et al.* [28] are very similar to the results of Mazzotta *et al.* [27], due to the similarity of the underlying atomic data used for these ion stages.

Ion-stage fractional abundances as a function of electron temperature for Ar^{9+}–Ar^{18+} are shown in Fig. 6. These ion stages are shown largely as a check on our calculations. We again show the results using our distorted-wave ionization and recombination data and compare with the tabulated fractional abundances of Bryans *et al.* [28]. The differences are relatively small. Our ionization balance calculation uses the same recombination data as Bryans *et al.* [28], but different ionization data. Bryans *et al.* [28] use the collisional ionization rate coefficients from Mazzotta *et al.* [27], which in turn are taken from a range of sources, mostly Arnaud and Rothenflug [44]. The good agreement between our ionization balance results and those of Bryans *et al.* [28] is due to the

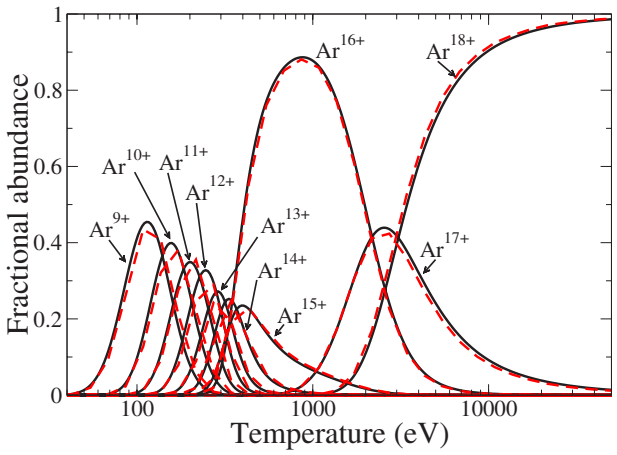

FIG. 6. (Color online) Equilibrium ion-stage balance for Ar^{9+}–Ar^{18+}. Solid line, our distorted-wave atomic data; dashed line, older atomic data [28].

dominance of direct ionization for ion stages above Ar^{7+}.

Therefore, the largest differences between our fractional abundances and literature values [27,28] are for the Ar–Ar^{7+} ion stages. The differences in the neutral and Ar^{+} ion stages are due mostly to the *R*-matrix with psuedostate ionization data that are used for neutral Ar and to the configuration-average distorted-wave dielectronic recombination data that is used for Ar^{+} recombining into neutral Ar. The differences in the remaining ion stages are mostly due to the dielectronic recombination data reported in this paper.

VI. SUMMARY

Electron-impact ionization cross sections and rate coefficients for Ar^{+}–Ar^{17+} were calculated using a configuration-average distorted-wave method. Generally good agreement was obtained between theoretical and experimental cross-section results for moderately charged ion stages. Electron-impact recombination cross sections and rate coefficients for Ar^{+}–Ar^{7+} were calculated using a configuration-average distorted-wave method. For temperatures above 10 eV, generally good agreement was obtained between the configuration-average and level-resolved distorted-wave rate coefficient results for Ar^{6+} and Ar^{7+}. Supplemented by recent *R*-matrix with pseudostate calculations for the ionization of neutral Ar [21] and level-resolved distorted-wave calculations for recombination from Ar^{8+} to Ar^{18+} [24,25,35–43], a complete atomic database was assembled to solve collisional equations for equilibrium ion stage fractional abundances along the entire Ar isonuclear sequence. The largest differences with previous ion-stage balance calculations [27,28] were found in the lower ion stages and could be attributed to differences in the ionization and recombination rate coefficients. In the future, we plan to extend level-resolved distorted-wave calculations for dielectronic recombination to the very complex *M*-shell atomic ions from Ar^{+} to Ar^{5+}. We also plan to apply the configuration-average distorted-wave method to study ion-stage balance along the heavy-element isonuclear sequences of interest to astrophysical and laboratory plasma research.

ACKNOWLEDGMENTS

This work was supported in part by a grant from the U.S. Department of Energy to Auburn University. Computational work was carried out at the National Energy Research Scientific Computing Center in Oakland, California.

[1] M. J. May, K. B. Fournier, D. Pacella, H. Kroegler, J. E. Rice, B. Gregory, M. Finkenthal, H. W. Moos, G. Mazzitelli, and W. H. Goldstein, Phys. Rev. E **61**, 3042 (2000).
[2] M. Mattioli, K. B. Fournier, L. Carraro, I. Coffey, G. Giroud, K. Lawson, P. Monier-Garbet, M. O'Mullane, J. Ongena, M. E. Puiatti, F. Sattin, P. Scarin, and M. Valisa, J. Phys. B **34**, 127 (2001).
[3] D. G. Whyte, T. C. Jernigan, D. A. Humphreys, A. W. Hyatt, C. J. Lasnier, P. B. Parks, T. E. Evans, M. N. Rosenbluth, P. L. Taylor, A. G. Kellman, D. S. Gray, E. M. Hollmann, and S. K. Combs, Phys. Rev. Lett. **89**, 055001 (2002).
[4] F. P. Keenan and S. M. McCann, J. Phys. B **23**, L423 (1990).
[5] J. Abdallah and R. E. H. Clark, J. Phys. B **27**, 3589 (1994).
[6] N. R. Badnell, Astrophys. J. Lett. **651**, L73 (2006).
[7] K. F. Man, A. C. H. Smith, and M. F. A. Harrison, J. Phys. B **20**, 5865 (1987).
[8] H. Gao, D. Fang, F. Lu, J. Gu, W. Wu, W. Hu, Y. Wang, J. Tang, and F. Tang, Nucl. Instrum. Methods Phys. Res. B **132**, 364 (1997).
[9] K. F. Man, A. C. H. Smith, and M. F. A. Harrison, J. Phys. B **26**, 1365 (1993).
[10] A. Danjo, A. Matsumoto, S. Ohtani, H. Suzuki, H. Tawara, K. Wakiya, and M. Yoshino, J. Phys. Soc. Jpn. **53**, 4091 (1984).
[11] D. W. Mueller, T. J. Morgan, G. H. Dunn, D. C. Gregory, and D. H. Crandall, Phys. Rev. A **31**, 2905 (1985).
[12] A. Müller, E. Salzborn, R. Frodl, R. Becker, H. Klein, and H. Winter, J. Phys. B **13**, 1877 (1980).
[13] D. C. Gregory, P. F. Dittner, and D. H. Crandall, Phys. Rev. A **27**, 724 (1983).
[14] H. Zhang, S. Cherkani-Hassani, C. Belenger, M. Duponchelle, M. Khouilid, E. M. Oualim, and P. Defrance, J. Phys. B **35**, 3829 (2002).
[15] D. H. Crandall, R. A. Phaneuf, and D. C. Gregory, ORNL-TM Rep. **9**, 501 (1985).
[16] A. M. Howald, D. C. Gregory, F. W. Meyer, R. A. Phaneuf, A. Müller, N. Djuric, and G. H. Dunn, Phys. Rev. A **33**, 3779 (1986).
[17] Y. Zhang, C. B. Reddy, R. S. Smith, D. E. Golden, D. W. Mueller, and D. C. Gregory, Phys. Rev. A **45**, 2929 (1992).
[18] S. Rachafi, D. S. Belic, M. Duponchelle, J. Jureta, M. Zambra, Z. Hui, and P. Defrance, J. Phys. B **24**, 1037 (1991).
[19] M. S. Pindzola, D. C. Griffin, and C. Bottcher, Phys. Rev. A **33**, 3787 (1986).
[20] Z. Altun (private communication).

[21] C. P. Ballance, D. C. Griffin, M. S. Pindzola, and S. D. Loch, J. Phys. B **40**, F27 (2007).
[22] Z. Altun, A. Yumak, N. R. Badnell, J. P. Colgan, and M. S. Pindzola, Astron. Astrophys. (to be published).
[23] Z. Altun, A. Yumak, N. R. Badnell, S. D. Loch, and M. S. Pindzola, Astron. Astrophys. **447**, 1165 (2006).
[24] N. R. Badnell, M. G. O'Mullane, H. P. Summers, Z. Altun, M. A. Bautista, J. Colgan, T. W. Gorczyca, D. M. Mitnik, M. S. Pindzola, and O. Zatsarinny, Astron. Astrophys. **406**, 1151 (2003).
[25] N. R. Badnell, Astrophys. J., Suppl. Ser. **167**, 334 (2006).
[26] H. P. Summers and M. G. O'Mullane, in *Nuclear Fusion Research*, edited by R. E. H. Clark and D. H. Reiter (Springer, Berlin, 2005), p. 399.
[27] P. Mazzotta, G. Mazzitelli, S. Colafrancesco, and N. Vittorio, Astron. Astrophys., Suppl. Ser. **133**, 403 (1998).
[28] P. Bryans, N. R. Badnell, T. W. Gorczyca, J. M. Laming, W. Mitthumsiri, and D. W. Savin, Astrophys. J., Suppl. Ser. **167**, 343 (2006).
[29] M. S. Pindzola, D. C. Griffin, and C. Bottcher, in *Atomic Processes in Electron-Ion and Ion-Ion Collisions*, Vol. 145 of NATO Advanced Studies Institute, Series B: Physics, edited by F. Brouillard (Plenum, New York, 1986), p. 75.
[30] S. D. Loch, M. S. Pindzola, C. P. Ballance, D. C. Griffin, D. M. Mitnik, N. R. Badnell, M. G. O'Mullane, H. P. Summers, and A. D. Whiteford, Phys. Rev. A **66**, 052708 (2002).
[31] S. D. Loch, J. A. Ludlow, M. S. Pindzola, A. D. Whiteford, and D. C. Griffin, Phys. Rev. A **72**, 052716 (2005).
[32] D. C. Griffin, M. S. Pindzola, and C. Bottcher, Phys. Rev. A **31**, 568 (1985).
[33] R. D. Cowan, in *The Theory of Atomic Structure and Spectra* (University of California Press, Berkeley, 1981).
[34] S. S. Tayal and R. J. W. Henry, Phys. Rev. A **33**, 3825 (1986).
[35] O. Zatsarinny, T. W. Gorczyca, K. T. Korista, N. R. Badnell, and D. W. Savin, Astron. Astrophys. **412**, 587 (2003).
[36] J. Colgan, M. S. Pindzola, A. D. Whiteford, and N. R. Badnell, Astron. Astrophys. **412**, 597 (2003).
[37] O. Zatsarinny, T. W. Gorczyca, K. T. Korista, N. R. Badnell, and D. W. Savin, Astron. Astrophys. **417**, 1173 (2004).
[38] J. Colgan, M. S. Pindzola, and N. R. Badnell, Astron. Astrophys. **417**, 1183 (2004).
[39] Z. Altun, A. Yumak, N. R. Badnell, J. Colgan, and M. S. Pindzola, Astron. Astrophys. **420**, 775 (2004).
[40] O. Zatsarinny, T. W. Gorczyca, K. Korista, N. R. Badnell, and D. W. Savin, Astron. Astrophys. **426**, 699 (2004).
[41] D. M. Mitnik and N. R. Badnell, Astron. Astrophys. **425**, 1153 (2004).
[42] O. Zatsarinny, T. W. Gorczyca, J. Fu, K. T. Korista, N. R. Badnell, and D. W. Savin, Astron. Astrophys. **447**, 379 (2006).
[43] N. R. Badnell, Astron. Astrophys. **447**, 389 (2006).
[44] M. Arnaud and R. Rothenflug, Astron. Astrophys., Suppl. Ser. **60**, 425 (1985).